RSC Advances

PAPER

View Article Online
View Journal | View Issue

Cite this: *RSC Adv.*, 2023, **13**, 4096

Solvent-dependent fluorescence behaviour of imide-fused [*n*]phenacenes (*n* = 3, 5, 7)†

Keito Nose,[a] Kaito Yoshioka,[a] Minoru Yamaji,[b] Fumito Tani,[c] Kenta Goto[c] and Hideki Okamoto *[ad]

Received 6th December 2022
Accepted 23rd January 2023

DOI: 10.1039/d2ra07771j

rsc.li/rsc-advances

Imide-fused [*n*]phenacenes (***n*PDIs**, *n* = 3, 5, 7) were systematically synthesised and their electronic features were investigated by electrochemical and electronic spectral measurements. ***n*PDIs** showed two reduction waves attributed to formation of radical ions and dianions. **3PDI** produced blue fluorescence independent of solvent polarity. In contrast, **5PDI** and **7PDI** displayed marked positive solvatofluorochromism due to intramolecular charge transfer characters between the imide moieties and phenacene π cores in the excited state. The spectral features were analyzed by the Lippert–Mataga relationship and theoretical calculations.

Introduction

[*n*]Phenacenes are polycyclic aromatic hydrocarbons (PAHs) consisting of a zigzag alignment of *n* benzene rings. These are referred to as one-dimensional graphene ribbons with armchair edges. Although phenacenes are chemically quite stable and robust, they have attracted less interest as functional materials because of their low solubility, low fluorescence efficiency and low light absorbing ability in the visible region.[1–3] Conventionally, π-extended [*n*]phenacenes, *i.e.* $n \geq 5$, have received little attention in functional chemistry and materials chemistry. Meanwhile, it was found that large phenacenes served as high-performance p-channel semiconductors and even as aromatic superconductors.[4,5] The results have opened the door to the material sciences of phenacenes, namely in organic electronics.[6,7]

Recently, the electronic properties and unprecedented optical characteristics of large phenacenes have been revealed; *e.g.*, picene ([5]phenacene) displayed fluorescence from the second excited state (S_2) in the vapour phase, a [2,2](5,8)picenophane derivative showed an exciplex fluorescence band and tetraester-functionalised [12]phenacene behaved as a unique nematogen, emitting polarised fluorescence from monomeric and dimeric forms.[8–10] It is thus expected that phenacenes would be a promising platform for constructing novel functional luminophores.

Imide-fused PAHs, typified by rylene diimides and acene diimides, have been extensively utilised as n-type organic electronic molecules, efficient fluorophores and supramolecular components.[11–13] In particular, synthesis and elucidation of electronic natures of rylene-diimide based functional molecules are one of the central topics in current fundamental and materials sciences.[14–16] Additionally, diverse molecular designs of polycyclic aromatic molecules are proposed and their electronic and optical properties are extensively explored. An imide fused fluoranthene, symmetrically combined with anthracene core, was reported to be solvatfluorochromic.[17] A naphthalimide derivative, substituted with two different functionalities on the imide moieties, showed fluorescence colour changes by interacting with aromatic solvents through exciplex formation.[18] Helicene and the related helical diimides provide optical properties due to the intra-molecular conjugation between the imide functionalities.[19,20]

In contrast to such established aromatic imide compounds, there are only a few studies on phenacenes incorporating imide functionalities. Previously reported imide-fused phenacenes have imide functionalities in the branching direction of the molecular axis because of the limited synthetic protocols.[21] A fulminene ([6]phenacene) diimide was reported to provide a fluorescence band with a maximum at 500 nm.[22] Extremely π-extended phenacene diimides exhibit an absorption band in a 450–470 nm region that is little dependent on numbers of the benzene rings involved in the molecules.[23] We recently synthesized picenes bearing imide moieties in the long molecular axis directions, **C_n-PicDIs** (see Fig. 1 for the chemical structure), and revealed that they served as n-channel organic semiconductors and displayed fluorescence band in the deep blue region.[24]

[a]*Division of Molecular Sciences, Graduate School of Natural Science and Technology, Okayama University, Okayama 700-8530, Japan. E-mail: hokamoto@okayama-u.ac.jp*
[b]*Division of Molecular Science, Graduate School of Science and Engineering, Gunma University, Ota 373-0057, Japan*
[c]*Institute for Materials Chemistry and Engineering, Kyushu University, Fukuoka 819-0395, Japan*
[d]*Department of Chemistry, Faculty of Natural Science and Technology, Okayama University, Okayama 700-8530, Japan*

† Electronic supplementary information (ESI) available: Synthetic procedures, NMR spectra of the new compounds, theoretical calculation results. See DOI: https://doi.org/10.1039/d2ra07771j

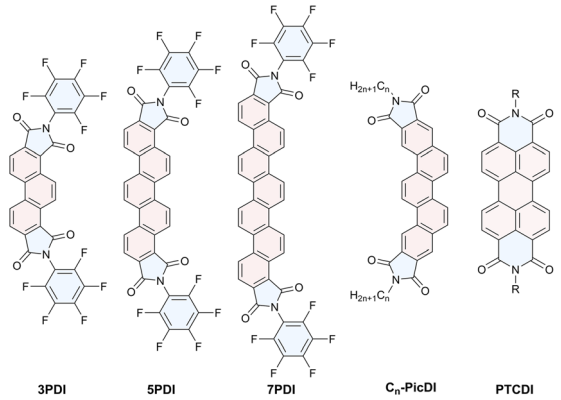

Fig. 1 Chemical structures of *n*PDIs and the related aromatic diimides.

Due to chemical stability and robustness, efficient functional dyes would be constructed employing the phenacene π core through an appropriate molecular design, *e.g.*, proper imidation. However, little is known about active manipulation of the electronic and spectral features of functionalised phanacenes. Therefore, we aimed to produce a phenacene-based functional dye. In this study, we synthesised [*n*]phanacene derivatives, ***n*PDIs** ($n = 3$, 5 and 7, see Fig. 1 for the chemical structures), incorporating imide functionalities at both edges of the molecules. The electronic features of ***n*PDIs** investigated by electrochemical and photophysical measurements are described, namely, it has been revealed that fluorescence behaviour of ***n*PDIs** can be effectively manipulated by solvent polarity.

Synthesis of *n*PDIs

To construct phenacene frameworks, the Mallory photoreaction of diarylethenes is one of the most efficient and reliable methods.[25] We have fully taken advantages of this strategy in the final step to effectively obtain ***n*PDIs** (Scheme 1). Pentafluorophenyl moieties have been introduced to enhance the electron-attracting ability of imide functionality.[26]

Diarylethene precursors **3**, **6** and **8** were prepared by either Wittig alkene synthesis between the appropriate arylaldehyde and arymethylphosphonium salt (for precursors **3** and **6**) or Migita–Kosugi–Stille coupling[27] between distannylethene and bromoarene **7** (for precursor **8**). These precursors were illuminated with black-light lamps (352 nm), in the presence of a catalytic amount of I_2, producing the desired ***n*PDIs** in moderate to good yields, **3PDI** (95%), **5PDI** (76%) and **7PDI** (40% from **7**). The detailed synthetic procedures of ***n*PDIs** and the intermediate building blocks, and their compound data are deposited in the ESI.†

Electrochemical characterization of *n*PDIs

To reveal the electronic features of ***n*PDIs**, electrochemical measurements were carried out using cyclic voltammetry (CV) and square wave voltammetry (SWV) techniques (Fig. 2). **3PDI** and **5PDI** showed two reversible reduction peaks in CV owing to the formation of radical anion and dianion species, as in the case of the reported rylene diimides.[28] **7PDI** showed a single

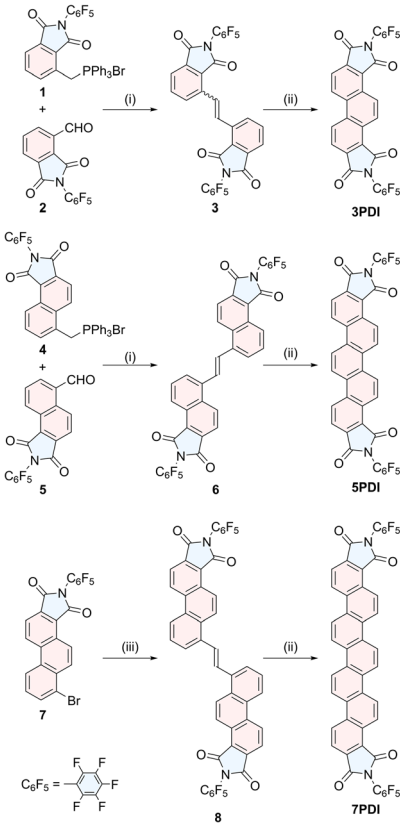

Scheme 1 Synthetic routes to *n*PDIs. Reagents and conditions: (i) Bu_4NF, CH_2Cl_2, (ii) *hν*, I_2, air, toluene, (iii) K_2CO_3, Bu_4NBr, CH_2Cl_2–THF then Bu_4NF, (iv) (*E*)-1,2-bis(tetrabutylstannyl)ethene, $Pd(PPh_3)_4$.

reduction peak; the two reduction waves were considered to be merged into one reduction wave. Such electrochemical behaviour was similar to that reported for aromatic diimides.[28,29] The first reduction potential (E_{red1}) was estimated to be −1.37, −1.49 and −1.54 V (*vs.* Fc/Fc^+) for **3PDI**, **5PDI** and **7PDI**, respectively. The electron affinity of the ***n*PDI** series was higher for the smaller homologue because the radical anion form of the smaller ***n*PDI** was more effectively stabilized by the two imide moieties in proximity. As for the second reduction potential (E_{red2}), the order is inverted: −1.66, −1.60 and −1.54 V (*vs.* Fc/Fc^+) for **3PDI**, **5PDI** and **7PDI**, respectively. It is considered that the negative charges distributed to the two imide moieties in the dianions of ***n*PDIs**, produced during two successive one-

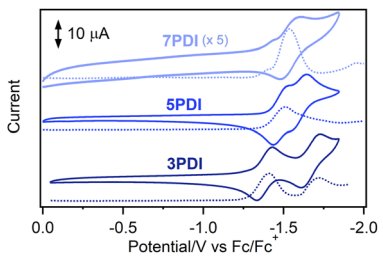

Fig. 2 CV (full lines) and SWV (dotted lines) curves for *n*PDIs observed in benzonitrile, in the presence of Bu_4NPF_6 (0.1 M).

electron reduction processes, led to repulsive coulombic interactions in the smaller homologue, namely, **3PDI**.[28] The energy levels of the lowest unoccupied molecular orbitals (LUMO, E_{LUMO}) were estimated to be −3.43, −3.31 and −3.26 eV for **3PDI**, **5PDI** and **7PDI**, respectively [$E_{LUMO} = -(4.8 + E_{red1})$ eV].[30] The E_{LUMO} values were slightly higher than those of related picene diimides (E_{LUMO} = *ca.* −3.9 eV)[24] indicating that the imide-fusing position affected the electron accepting ability.

Electronic spectra

The electronic spectral characteristics of ***n*PDIs** were investigated by absorption and fluorescence spectral measurements in various solvents (Fig. 3), and the photophysical parameters are summarised in Table 1. ***n*PDIs** showed a small absorption band in the longer wavelength region (400–450 nm). The absorption band slightly red shifted upon increasing the number of fused benzene rings from $n = 3$ to 5, and λ_{abs} values of **5PDI** and **7PDI** were similar to each other; λ_{abs} = 404–409 nm for **3PDI**, 428–434 nm for **5PDI**, 423–431 nm for **7PDI** (*cf.* Fig. S6 in the ESI†). The entire absorption spectral profiles for each ***n*PDIs** were almost independent of the solvent polarity.

In fluorescence spectra, **3PDI** displayed an emission band in the 400–600 nm region. The emission band was essentially insensitive to solvent polarity (Fig. 3a). In DMSO, no fluorescence emission of **3PDI** was detected. For **5PDI** and **7PDI**, the fluorescence band was significantly sensitive to solvent polarity and bathochromically shifted depending on solvent polarity (Fig. 3b and c). As a result, the fluorescence colour changed from blue (λ_{FL} = 454 nm in toluene) to yellow (λ_{FL} = 533 nm in DMSO) for **5PDI**, and from sky blue (λ_{FL} = 482 nm in toluene) to orange (λ_{FL} = 581 nm in DMSO) for **7PDI**.

Regardless of the solvent used, the fluorescence quantum yield of **3PDI** (Φ_F = *ca.* 0.15) was slightly higher than that of parent phenanthrene (Φ_F = 0.049 in aerated $CHCl_3$).[3] The Φ_F values of **5PDI** and **7PDI** were, respectively, determined to be 0.32 and 0.35 in toluene, which were about 4-fold larger than that for parent picene (Φ_F = 0.088 in aerated $CHCl_3$).[3] Upon increasing solvent polarity, the Φ_F values tended to decrease. These results suggest that the lowest excited states (S_1) of **5PDI** and **7PDI** are of intramolecular charge transfer (ICT) nature.

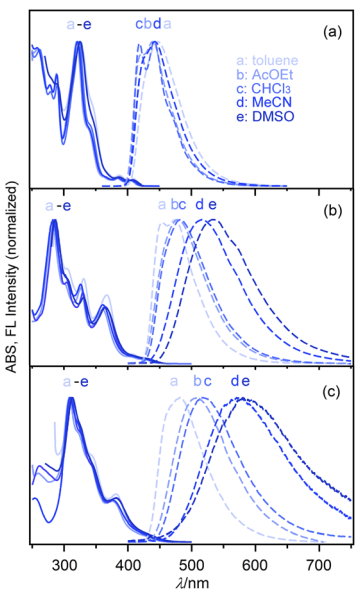

Fig. 3 Electronic absorption (full lines) and fluorescence spectra (dashed lines) of ***n*PDIs** in various solvents: (a) 3PDI, (b) 5PDI and (c) 7PDI.

Table 1 Photophysical parameters for ***n*PDIs**

Compound	Solvent	λ_{abs} (nm)	λ_{FL}[a] (nm)	$\Delta\tilde{\nu}$[b] (cm^{-1})	Φ_F[c]
3PDI	Toluene	409	429[d]	863	0.17
	$CHCl_3$	409	417[d]	485	0.11
	AcOEt	404	415[d]	677	0.15
	MeCN	405	419[d]	836	0.17
	DMSO	408	—[e]	—[e]	—[e]
5PDI	Toluene	428	454	1340	0.32
	$CHCl_3$	434	483	2340	0.26
	AcOEt	429	478	2390	0.15
	MeCN	430	516	3880	0.29
	DMSO	433	533	4330	0.07
7PDI	Toluene	429[d]	482	2580	0.35
	$CHCl_3$	431[d]	515	3790	0.28
	AcOEt	423[d]	510	4020	0.30
	MeCN	430[d]	571	5740	0.10
	DMSO	430[d]	581	6040	0.08

[a] Fluorescence excitation spectra were consistent with absorption spectra (Fig. S1–S3 in ESI). [b] Stokes shift. [c] Fluorescence quantum yield determined under aerated conditions. [d] The positions of the 0–0 band were estimated from simulated spectra by peak fitting (Fig. S4 and S5, in ESI). [e] No detectable fluorescence emission was observed.

The solvatofluorochromic behaviour of ***n*PDIs** was analysed using the Lippert–Mataga relationship (eqn (1)),[31,32]

$$\Delta\tilde{\nu} = \tilde{\nu}_A - \tilde{\nu}_F = \frac{2\Delta\mu^2}{hca_0{}^3}\Delta f + \text{const}, \quad (1)$$

$$\Delta f = \frac{\varepsilon_r - 1}{2\varepsilon_r + 1} - \frac{n^2 - 1}{2n^2 + 1}, \quad (2)$$

where $\Delta\tilde{\nu}$ is the Stokes shift estimated by the difference in peak wavenumbers between the absorption and fluorescence emission bands (*cf.* Fig. S4 and S5 in the ESI†), h is the Planck constant, c is the velocity of light in vacuum, $\Delta\mu$ is the dipole moment change between the ground and excited states, a_0 is the Onsagar cavity radius and Δf is the orientation polarizability of solvents expressed by dielectric constant (ε_r) and refractive index (n) of the solvents (eqn (2)). The Lippert–Mataga plots showed linear correlations (Fig. 4) and the $\Delta\mu$ values were estimated from the slopes; $\Delta\mu$ = 4.8 D for **3PDI**, 11.3 D for **5PDI** and 13.8 D for **7PDI**. It was, thus, revealed that **3PDI** showed little change in dipole moment upon excitation whereas **5PDI** and **7PDI** were significantly polarised in the S_1 state.

In the case of related picene diimide, **C_8-PicDI**, the solvatofluorochromic shift was substancially less significant (λ_{FL} = 412 nm in toluene, λ_{FL} = 425 nm in DMSO, Fig. S7a in the ESI†) compared to that of **5PDI** (λ_{FL} = 428 nm in toluene, λ_{FL} = 533 nm in DMSO, Table 1). It can be concluded that the imide-fusing positions play an important role for inducing the solvent-

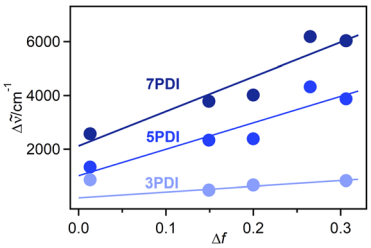

Fig. 4 Lippert–Mataga plots for *n*PDIs. The point for **3PDI** in toluene ($\Delta f = 0.013$) was omitted as it deviated from the linear correlation. The Δf values were calculated by eqn (2). The n and ε_r values were obtained from ref. 33.

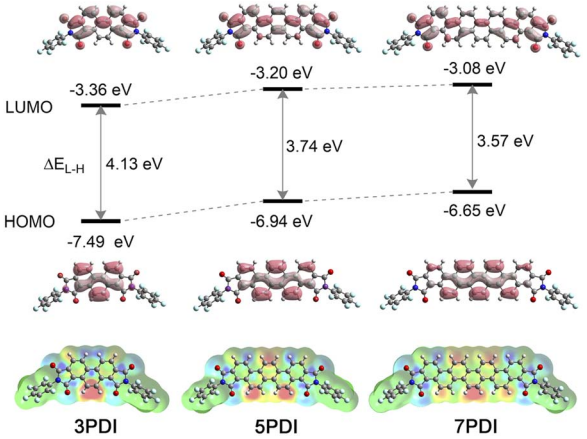

Fig. 5 Upper: Frontier molecular orbital diagrams of *n*PDIs. The calculated energy levels of HOMO and LUMO, and HOMO–LUMO energy gap (ΔE_{L-H}) are shown. Lower: Density difference mappings for S_0–S_1 electronic transition; the red regions indicate reduced electron density and the blue regions indicate increased electron density upon the photoexcitation.

dependent fluorescence behaviour. Additionally, only slight solvent-dependent electronic spectral shift of **PTCDI** (R = octyl) was observed indicating that the perylene diimide, incorporating no substituent on the aromatic core, insignificantly responded to solvent environments (Fig. S7b in the ESI†).

It would be worth mentioning that **3PDI** displayed fluorescence behaviour different form that of **5PDI** and **7PDI**. The fluorescence band observed in toluene was apparently broadened and its onset wavelength slightly red shifted compared to that observed in the other solvent. Additionally, in DMSO, the fluorescence of **3PDI** was totally quenched, whereas that of **5PDI** and **7PDI** did not vanish. A Stern–Volmer plot for the fluorescence quenching of **3PDI** with DMSO apparently showed a linear relationship in a low DMSO concentration region (<75 mM, Fig. S8 in the ESI†). It is considered that there is a specific interaction between **3PDI** and DMSO molecules through a dynamic process. DMSO has been shown to cause fluorescence quenching of ICT fluorophores *via* specific mechanisms such as hydrogen bonding and improved twisted intramolecular charge transfer (TICT).[34,35] However, in the case of **3PDI**, such mechanisms could be excluded as **3PDI** has no hydrogen donor and the pentafluorophenyl moieties would not contribute to the frontier orbitals (*cf.* Fig. 5). It has been mentioned that DMSO quenched fluorescence of Zn-bis(dipyrromethenate)s through coordination-mediated interactions and/or photo-induced electron transfer (PET).[36] In the case of **3PDI**-DMSO system, fluorescence quenching through a PET mechanism might be an alternative possibility. The detailed quenching mechanism is currently not clear and is being investigated.

Theoretical analyses

To further obtain insights into the electronic features of the excited state of ***n*PDI**s, theoretical analyses were carried out at the (TD) PBE0/6-311+G(2df,2p) level of theory.[37] Fig. 5 shows the calculated frontier molecular orbitals and energy levels, and density difference mapping corresponding to the electronic transition from the S_0 to S_1 states. The energy gap for the highest occupied molecular orbitals (HOMO) and LUMO (ΔE_{L-H}) gradually decreases with increasing benzene ring numbers in ***n*PDI**s.

The molecular orbital diagrams of the HOMO display similar features for the ***n*PDI** series, *i.e.*, the HOMO is localised exactly on the phenacene cores. In contrast, the LUMO was delocalised over the entire molecules extending to the two imide moieties. The LUMO energy levels (E_{LUMO}) increased with the increasing number of fused benzene rings in ***n*PDI**s. It is reasonable to consider that, for **3PDI**, more efficient conjugation between the phenanthrene core and electron-accepting imide moieties more effectively stabilises the LUMO compared to larger ***n*PDI**s. The order of the calculated E_{LUMO} values was consistent with that of the first reduction potentials estimated by electrochemical measurements (Fig. 2).

The excited state natures of ***n*PDI**s were investigated in vacuum using the TD-DFT method. The calculated transition wavelengths [$\lambda(S_0$–$S_1)$], oscillator strengths (f) and configurations of the electronic transitions are summarized in Table S1 in the ESI.† Additionally, the calculated absorption spectra were compared with the experimental absorption spectra recorded in $CHCl_3$ (Fig. S9 in the ESI†). The calculation results slightly overestimated the transition energies compared with the experimentally observed absorption spectra. The S_1 state is mainly attributed to the HOMO–LUMO transition for all ***n*PDI**s (Table S1 in the ESI†). Based on the results that the HOMO is located on the phenacene cores and the LUMO expands to the two imide moieties (Fig. 5), the S_1 state of ***n*PDI**s is considered to possess ICT properties between the phenacene π core and imide functionality.

The density difference mappings for the S_0–S_1 electronic transition (Fig. 5, lower) provide additional insight into the ICT characteristics of ***n*PDI**s in the S_1 state. Upon excitation, the electron density at the peripheral double bonds in the central phenacene cores decreased (red regions), whereas that at the imide carbonyl moieties increased (blue regions). Consequently, in the cases of **5PDI** and **7PDI**, an enhanced electronic dipole moment was induced in the S_1 state resulting in appreciable positive solvatofluorochromism. In the case of **3PDI**, the two negatively charged imide moieties opposed the positively

charged double bond. They behave like quasi-quadrupoles to reduce the polarized character of the entire molecule in the S_1 state. Thus, **3PDI** showed minimal fluorescence response to solvent polarity.

Conclusions

A series of imide-fused phenacenes ***n*PDI**s was photochemically synthesized and their electronic features were electrochemically and photophysically investigated. The E_{LUMO} of **5PDI** estimated from the electrochemical measurements, −3.31 eV, was slightly higher than that of related **C_n-PicDI**, *ca.* −3.9 eV. The results suggested that electron accepting ability of imide-fused phenacenes can be manipulated by the position of the imide functionalities. Due to the ICT characters between the phenacene π-core and the imide moieties, **5PDI** and **7PDI** displayed marked positive solvatofluorochromism. **3PDI** displayed negligible solvent effects on fluorescence and showed effective quenching in DMSO. The present results provide a novel strategy for developing fluorophores utilising [*n*]phenacenes, specifically $n \geq 5$, which have rarely been used in development of luminescent functional materials. To our knowledge, **5PDI** and **7PDI** provide the first phanacene-based fluorophores responding to solvent environments, and their A–D(π)–A electronic alignment would be potentially applicable to non-linear optics.[38]

Author contributions

Keito Nose: investigation, validation. Kaito Yoshioka: investigation, validation. Minoru Yamaji, investigation, validation, writing–original draft. Fumito Tani: investigation, validation. Kenta Goto: investigation, validation. Hideki Okamoto: conceptualization, validation, writing–original draft.

Conflicts of interest

There are no conflicts to declare.

Acknowledgements

The present study was supported by Grants-in-Aid for Scientific Research, KAKENHI, from JSPS, Japan (JP18H02043 and JP20K05648), and by the Cooperative Research Program of the 'Network Joint Research Centre for Materials and Devices.'

Notes and references

1 F. B. Mallory, K. E. Butler, A. C. Evans, E. J. Brondyke, C. W. Mallory, C. Yang and A. Ellenstein, *J. Am. Chem. Soc.*, 1997, **119**, 2119–2124.
2 F. B. Mallory, K. E. Butler, A. C. Evans and C. W. Mallory, *Tetrahedron Lett.*, 1996, **37**, 7173–7176.
3 H. Okamoto, M. Yamaji, S. Gohda, K. Sato, H. Sugino and K. Satake, *Res. Chem. Intermed.*, 2013, **39**, 147–159.
4 H. Okamoto, N. Kawasaki, Y. Kaji, Y. Kubozono, A. Fujiwara and M. Yamaji, *J. Am. Chem. Soc.*, 2008, **130**, 10470–10471.
5 R. Mitsuhashi, Y. Suzuki, Y. Yamanari, H. Mitamura, T. Kambe, N. Ikeda, H. Okamoto, A. Fujiwara, M. Yamaji, N. Kawasaki, Y. Maniwa and Y. Kubozono, *Nature*, 2010, **464**, 76–79.
6 Y. Kubozono, X. He, S. Hamao, K. Teranishi, H. Goto, R. Eguchi, T. Kambe, S. Gohda and Y. Nishihara, *Eur. J. Inorg. Chem.*, 2014, 3806–3819.
7 Y. Kubozono, H. Mitamura, X. Lee, X. He, Y. Yamanari, Y. Takahashi, Y. Suzuki, Y. Kaji, R. Eguchi, K. Akaike, T. Kambe, H. Okamoto, A. Fujiwara, T. Kato, T. Kosugi and H. Aoki, *Phys. Chem. Chem. Phys.*, 2011, **13**, 16476–16493.
8 T. Itoh, M. Yamaji and H. Okamoto, *Chem. Phys. Lett.*, 2013, **570**, 26–28.
9 M.-C. Tang, Y.-C. Wei, Y.-C. Chu, C.-X. Jiang, Z.-X. Huang, C.-C. Wu, T.-H. Chao, P.-H. Hong, M.-J. Cheng, P.-T. Chou and Y.-T. Wu, *J. Am. Chem. Soc.*, 2020, **142**, 20351–20358.
10 G. Farias, D. S. Simeão, T. S. Moreira, P. L. dos Santos, A. Bentaleb, E. Girotto, A. P. Monkman, J. Eccher, F. Durola, H. Bock, B. de Souza and I. H. Bechtold, *J. Mater. Chem. C*, 2019, **7**, 12080–12085.
11 M. Al Kobaisi, S. V. Bhosale, K. Latham, A. M. Raynor and S. V. Bhosale, *Chem. Rev.*, 2016, **116**, 11685–11796.
12 Y. Avlasevich, C. Li and K. Müllen, *J. Mater. Chem.*, 2010, **20**, 3814–3826.
13 X. Zhan, A. Facchetti, S. Barlow, T. J. Marks, M. A. Ratner, M. R. Wasielewski and S. R. Marder, *Adv. Mater.*, 2011, **23**, 268–284.
14 W. Jiang and Z. Wang, *J. Am. Chem. Soc.*, 2022, **144**, 14976–14991.
15 S. Maniam, H. F. Higginbotham, T. D. M. Bell and S. J. Langford, *Chem.–Eur. J.*, 2019, **25**, 7044–7057.
16 A. Herrmann and K. Müllen, *Chem. Lett.*, 2006, **35**, 978–985.
17 H. Ishikawa, K. Katayama, J. Nishida, C. Kitamura and T. Kawase, *Tetrahedron Lett.*, 2018, **59**, 3782–3786.
18 M. Pandeeswar and T. Govindaraju, *RSC Adv.*, 2013, **3**, 11459–11462.
19 F. Saal, F. Zhang, M. Holzapfel, M. Stolte, E. Michail, M. Moos, A. Schmiedel, A.-M. Krause, C. Lambert, F. Würthner and P. Ravat, *J. Am. Chem. Soc.*, 2020, **142**, 21298–21303.
20 G. Zhang, J. Tan, L. Zhou, C. Liu, J. Liu, Y. Zou, A. Narita and Y. Hu, *Org. Lett.*, 2021, **23**, 6183–6188.
21 L. Sturm, F. Aribot, L. Soliman, H. Bock and F. Durola, *Eur. J. Org. Chem.*, 2022, e202200196.
22 R. Wang, K. Shi, K. Cai, Y. Guo, X. Yang, J.-Y. Wang, J. Pei and D. Zhao, *New J. Chem.*, 2016, **40**, 113–121.
23 T. S. Moreira, M. Ferreira, A. Dall'armellina, R. Cristiano, H. Gallardo, E. A. Hillard, H. Bock and F. Durola, *Eur. J. Org. Chem.*, 2017, 4548–4551.
24 Y. Guo, K. Yoshioka, S. Hamao, Y. Kubozono, F. Tani, K. Goto and H. Okamoto, *RSC Adv.*, 2020, **10**, 31547–31552.
25 F. B. Mallory and C. W. Mallory, *Org. React.*, 1984, **30**, 1–456.
26 T. Korenaga, K. Kadowaki, T. Ema and T. Sakai, *J. Org. Chem.*, 2004, **69**, 7340–7343.
27 V. Farina, V. Krishnamurthy and W. J. Scott, *Org. React.*, 1997, **50**, 1–652.

28 S. K. Lee, Y. Zu, A. Herrmann, Y. Geerts, K. Müllen and A. J. Bard, *J. Am. Chem. Soc.*, 1999, **121**, 3513–3520.
29 X. Zhao, Y. Xiong, J. Ma and Z. Yuan, *J. Phys. Chem. A*, 2016, **120**, 7554–7560.
30 H. Qu, W. Cui, J. Li, J. Shao and C. Chi, *Org. Lett.*, 2011, **13**, 924–927.
31 E. Lippert, *Z. Naturforsch.*, 1955, **10**, 541–545.
32 N. Mataga, Y. Kaifu and M. Koizumi, *Bull. Chem. Soc. Jpn.*, 1955, **28**, 690–691.
33 C. Reichardt, *Solvents and Solvent Effects in Organic Chemistry*, Wiley-VCH, Weinheim, 3rd edn, 2003.
34 A. Maliakal, G. Lem, N. J. Turro, R. Ravichandran, J. C. Suhadolnik, A. D. DeBellis, M. G. Wood and J. Lau, *J. Phys. Chem. A*, 2002, **106**, 7680–7689.
35 D. Cho and W. L. Mattice, *J. Phys. Chem.*, 1990, **94**, 3847–3851.
36 A. A. Ksenofontov, G. B. Guseva, E. V. Antina, I. A. Khodov and A. I. Vyugin, *Sens. Actuators, B*, 2017, **251**, 858–868.
37 C. Adamo and V. Barone, *J. Chem. Phys.*, 1999, **110**, 6158–6170.
38 O. Mongin, L. Porrès, M. Charlot, C. Katan and M. Blanchard-Desce, *Chem.–Eur. J.*, 2007, **13**, 1481–1498.